Squirrel-Cage Induction Motor Parameter Estimation using a Variable Frequency Test

Lluís Monjo, *Student Member, IEEE*, Hengameh Kojooyan-Jafari, Felipe Córcoles and Joaquín Pedra, *Member, IEEE*

***Abstract*-- This paper presents a method for squirrel-cage induction motor parameter estimation using a phase-to-phase standstill variable frequency test. The measured resistance and reactance at different frequencies are the data of the minimization error function to be minimized for single- and double-cage model parameters estimation. It is observed that the single-cage model is unable to fit the measured data for frequencies above several tenths of Hertz whereas the double-cage model fits the measured data accurately in all the frequency range (from 0 to 150 Hz). The single- and double-cage estimated parameters are validated by comparison with data from two additional tests: (1) steady-state torque and current measurement test at different speeds, (2) dynamic free-acceleration test. Again, the agreement between measured and predicted torque (in the first test) and current (in both tests) is satisfactory only for the double-cage model.**

***Index Terms*-- Induction motor, parameter estimation, standstill frequency response test.**

I. Introduction

Induction motor parameter estimation is an important topic in the electric drive literature because controller performance depends on the accuracy of the motor parameters used by the control algorithm. The usual method for squirrel-cage induction motor parameter estimation is based on no-load and locked rotor tests [1]. Many papers have been published on the single-cage model parameter estimation using steady-state, variable frequency and transient tests data [2]. Most variable frequency tests are carried out by supplying only two phases of the stator (namely, phase-to-phase tests) with a variable amplitude and variable frequency sinusoidal voltage source when the rotor speed is null; resulting in the so-called standstill frequency response (SSFR) tests (Fig. 1). These tests may use a controlled voltage source with tunable frequency or the PWM voltage waveform supplied by a drive inverter. As the torque in a phase-to-phase test is null, the SSFR test can be conducted during maintenance periods, when impact on plant operations is minimal. Ref. [3] proposes a phase-to-phase test using the PWM inverter at two different frequencies to determine the single-cage model parameters. In Ref. [4], an SSFR test for derivation of single-cage model parameters is conducted and the influence of skin and proximity effects on the rotor resistance is discussed. Ref. [5] proposes and compares a method with three other methods. Despite the good agreement obtained with steady-state measurements, the comparison with a free-acceleration test data shows poor accuracy, which is attributed to saturation. Ref. [6] proposes a frequency response test to determine the electrical parameters of an induction wind generator. Ref. [7] puts forward an automatic procedure for single-cage model parameter estimation. Reference [8] uses the SSFR to estimate the induction machine parameters with a genetic algorithm and its application to torque control. Finally, [9] deserves a special interest because it focuses on double-cage model parameter estimation with SSFR test.

The paper presents and compares the single- and double-cage model predictions when their parameters are estimated using SSFR measurements. Also, the steady-state torque- and current-speed curves predicted by both models are compared with those measured in the laboratory. Finally, the Park transformed currents measured in a free-acceleration test are compared with those predicted by the double-cage model.

II. Induction Motor Model

Fig. 2a shows the equivalent circuit of the single-cage model. This circuit has five different parameters. However, it is well established that only four are independent [10]. Hence, a relation between the parameters must be imposed, typically $X_{sd} = X_{rd}$ [11]. Fig. 2b illustrates the equivalent circuit of the double-cage model. This model has seven parameters, but only six are independent [11]. In this case, the relation $X_{sd} = X_{2d}$ is chosen.

The literature typically considers that X_{1d} and R_1 represent the inner cage, which has a predominant effect near rated speed, whereas X_{2d} and R_2 represent the outer cage, which has

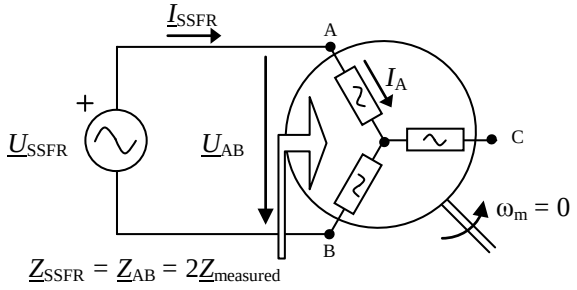

Fig. 1 Connection scheme for the SSFR test.

This research work has been supported by grant ENE2009-10274 and DPI2011-28021.

Ll. Monjo, H. Kojooyan-Jafari, F. Córcoles and J. Pedra are with the Department of Electrical Engineering, ETSEIB-UPC, Av. Diagonal 647, 08028 Barcelona, Spain (e-mails: lluis.monjo@upc.edu, kojooyan@iiau.ac.ir, corcoles@ee.upc.es, pedra@ee.upc.es).

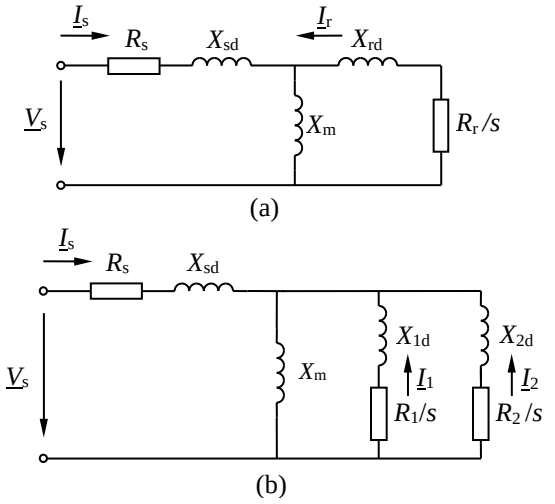

Fig. 2. Steady-state star equivalent circuit for the three-phase induction machine: a) single-cage model (five-parameter circuit), and b) double-cage model (seven-parameter circuit).

a predominant effect near zero speed.

The circles in Fig. 3 represent the steady-state torque and current of two ABB medium size motors measured by the manufacturer (the catalogue data is shown in Table I). Table II contains the single- and double-cage model parameters estimated from the previous manufacturer measurements. The curves predicted by both models are also plotted in Fig. 3. As expected, the double-cage model exhibits good agreement between measurements and predictions while the single-cage model provides accurate results only between synchronous speed and the point of maximum torque. This figure shows clearly that the squirrel-cage motor must be represented with the double-cage model [12]-[14].

TABLE I
CATALOGUE DATA OF TESTED SQUIRREL-CAGE INDUCTION MOTORS

	P_N (kW)	U_N (V)	f_N (Hz)	PF_N	ω_N (r/min)	η_N (%)	T_{MAX}/T_N	T_{ST}/T_N	I_{ST}/I_N
Motor #1	90	400	50	0.88	2965	94.0	2.7	2.0	6.3
Motor #2	45	400	50	0.83	1480	91.0	2.5	2.6	6.0
Motor #3	1.5	400	50	0.69	950	79.1	2.3	1.7	3.9
Motor #4	2.2	400	50	0.78	1450	86.0	4.6	4.0	8.5
Motor #5	2.2	400	50	0.71	940	78.0	2.3	1.9	4.5

It is worth noting that the predicted currents of the single-cage model in Fig. 3 are nearly constant for large values of slip (s > 0.8) while in the double-cage model they increase monotonically with the slip increase.

III. SIMULATED TREND OF THE MODELS' IMPEDANCE WITH FREQUENCY

The per-phase equivalent impedance of the single-cage model in Fig. 2a at zero speed and stator frequency f is

$$\underline{Z}_{\text{single-cage}}(f) = R_s + \mathrm{j}X_{sd} + \frac{1}{\dfrac{1}{\mathrm{j}X_m} + \dfrac{1}{R_r + \mathrm{j}X_{rd}}} \qquad (1)$$

The impedance of the double-cage model in Fig. 2b at zero speed and stator frequency f is

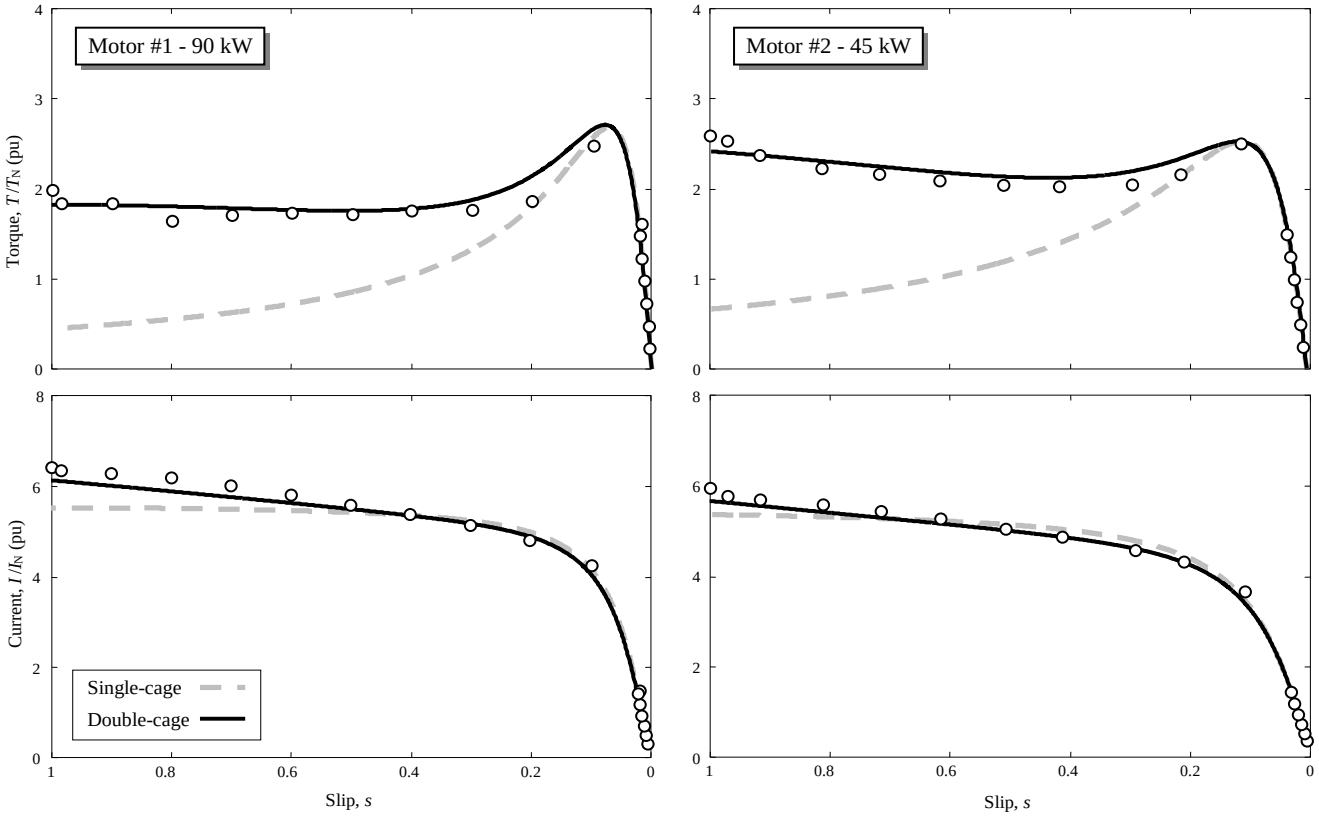

Fig. 3. TIS test: measured and predicted (single- and double-cage models) torque- and current- slip curves for the motors #1 and #2.

TABLE II
ESTIMATED PARAMETERS FOR THE SINGLE- AND DOUBLE-CAGE MODELS IN PU ($S_B = P_N$, $U_B = U_N$, $Z_B = U_B^2 / S_B$)

	Single-cage model from TIS tests					Double-cage model from TIS tests						
	r_s	x_{sd}	x_m	r_r	x_{rd}	r_s	x_{sd}	x_m	r_1	x_{1d}	r_2	x_{2d}
Motor #1	0.0334	0.0710	3.3102	0.0101	0.0710	0.0334	0.0582	3.1176	0.0117	0.0976	0.1325	0.0582
Motor #2	0.0430	0.0684	1.8564	0.0153	0.0684	0.0430	0.0366	2.1718	0.0170	0.1205	0.1474	0.0366

$$\underline{Z}_{\text{double-cage}}(f) = R_s + jX_{sd} + \frac{1}{\frac{1}{jX_m} + \frac{1}{R_1 + jX_{1d}} + \frac{1}{R_2 + jX_{2d}}} \quad (2)$$

If the stator frequency f is different from rated (f_N) and the machine reactances have been initially calculated at rated frequency, they must be corrected to be used in (1)-(2):

$$X = X_N \left(\frac{f}{f_N} \right) \quad (3)$$

In the rest of the paper, the resistance $R(f)$ and the reactance $X(f)$ will be the real and imaginary part of the per-phase machine equivalent impedance:

$$\underline{Z}(f) = R(f) + jX(f) \quad (4)$$

The evolution of $R(f)$ and $X(f)$ for the single- and double-cage models of motor #2 (Table II) when frequency varies from 0.5 to 150 Hz is simulated and shown in Fig. 4. Fig. 4c illustrates a vertical zoom of the $R(f)$ resistance curves of both models. From this figure, two important features are evident: (1) the resistance curves of both models exhibit identical behavior in the low frequency range; (2) the resistance curve of the single-cage model is nearly constant at high frequencies (150 Hz) while the curve of the double-cage model continues increasing.

The limit value of $R_{\text{single-cage}}$ at high frequencies obtained from the real part of (1) is

$$R_{\text{single-cage}}(\infty) = R_s + \lim_{f \to \infty} \frac{X_m^2 R_r - X_m X_{rd} R_r}{R_r^2 + (X_m + X_{rd})^2} = \\ = R_s + \left(\frac{M}{M + L_{rd}} \right)^2 R_r \approx R_s + R_r \quad (5)$$

This result proves that the single-cage machine resistance is nearly constant at high frequencies.

IV. LABORATORY TESTS

Three different squirrel-cage induction motors (motors #3, #4, and #5 in Table I) were tested in the authors laboratory. The test setup consisted of the following parts: a) loading machine and speed controller (DC machine and DC adjustable speed drive); b) torque transducer mounted on the motor axis and speed and current sensors; c) variable three-phase source, and d) induction motor.

To estimate and validate the parameters of the squirrel-cage induction motor, three different tests were performed:

1. Phase-to-phase standstill frequency response test (SSFR) at a rated current.
2. Steady-state three-phase test at rated frequency and constant reduced voltage and at different speeds (TIS).
3. Free-acceleration test at rated frequency and constant reduced voltage.

The test purposes and variables are summarized in Table III.

As the steady-state current at a given large slip is several times rated, the machine temperature rises if the machine continuously operates at such large slip. As a consequence, the

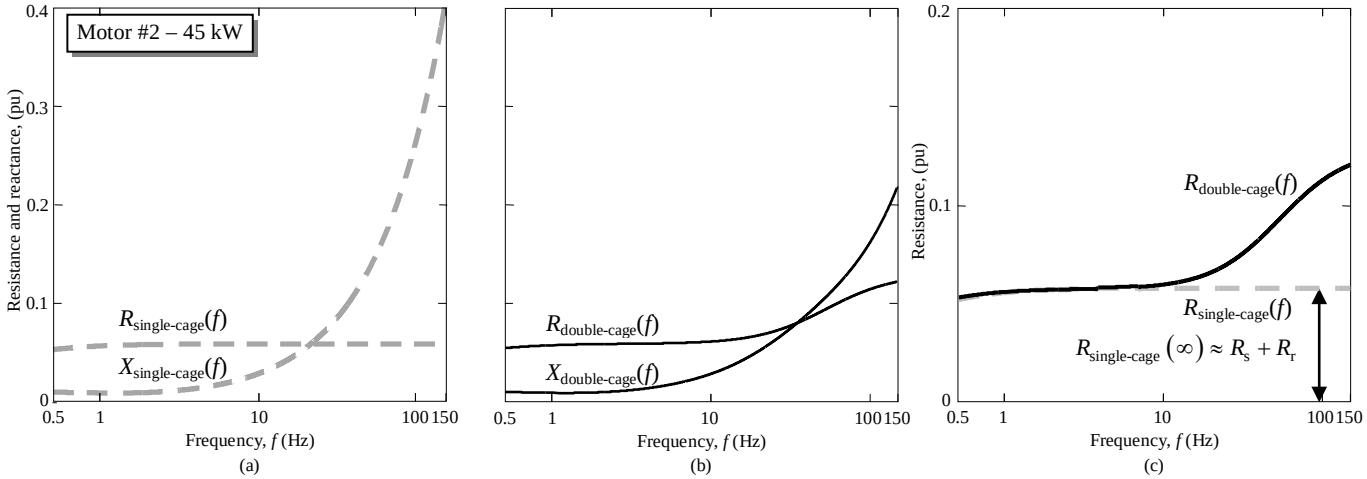

Fig. 4. SSFR test: simulated phase resistance and reactance for motor #2. (a) single- and (b) double-cage models, and (c) vertical zoom of the resistance curves of both models.

TABLE III
PURPOSE AND VARIABLES INVOLVED IN THE LABORATORY TESTS

	Test	Purpose	Phases	v_{sa}	v_{sb}	v_{sc}	i_{sa}	i_{sb}	i_{sc}	ω_m	Torque	Figures
1)	Variable frequency, SSFR	Estimation	Phase-to-phase	✓	✓	×	✓	✓	×	×	×	5 and 6
2)	Steady-state, TIS	Estimation and validation	Three-phase	✓	✓	✓	✓	✓	✓	✓	✓	7 and 8
3)	Free-acceleration	Validation	Three-phase	✓	✓	✓	✓	✓	✓	✓	×	9

winding resistance increases. For this reason, the steady-state measures in Fig. 3 were taken by assuring that the stator resistance was keep constant. It is assumed that keeping constant the stator resistance also keeps constant the rotor resistance. This fact is not very important in the free-acceleration test, because the large starting currents are vanished within a few milliseconds.

A. Saturation Influence Elimination

To avoid the leakage reactances saturation influence [15] and successfully compare SSFR measurements with TIS and free-acceleration tests measurements, special attention must be paid to the stator currents because the leakage reactances saturation depends on their currents. As similar current values result in similar saturation levels, the next restrictions have been imposed to the supplied voltage and currents in these tests:

- SSFR test: the stator current at any frequency was fixed to the nominal current (so, the stator voltage at any frequency was different).
- TIS and free-acceleration tests: the stator voltage at any test was fixed to the reduced voltage that produces the nominal current at zero speed (so, the stator current at any test was different).

B. Measured Tests Normalization to the Rated Voltage

Torque and current were prorated to rated voltage to make the different tests comparable:

$$T_{\text{prorated}} = T_{\text{measured}} \left(\frac{U_{\text{N}}}{U} \right)^2 \quad ; \quad I_{\text{prorated}} = I_{\text{measured}} \left(\frac{U_{\text{N}}}{U} \right) \tag{6}$$

where U_N is the nominal value.

V. SSFR TEST

The circuit in Fig. 2 also represents the direct sequence circuit of the motor. The inverse sequence circuits are identical, but the slip s is replaced in both circuits by the term $(2 - s)$. The direct, $\underline{Z}_d$, and inverse, $\underline{Z}_i$, impedances match up at zero speed, as $s = 1$ and $2 - s = 1$:

$$\underline{Z}_{\text{d}}(s=1) = \underline{Z}_{\text{i}}(s=1) \tag{7}$$

As justified in the Appendix, the motor impedance at slip s when only two phases are supplied (namely, phases A and B) is:

$$\underline{Z}_{\text{AB}} = \underline{Z}_{\text{d}}(s) + \underline{Z}_{\text{i}}(s) \tag{8}$$

As the speed is null and only two phases are supplied the equations (7) and (8) give the test impedance $\underline{Z}_{\text{SSFR}}$:

$$\underline{Z}_{\text{SSFR}} = \underline{Z}_{\text{AB}} = \underline{Z}_{\text{d}}(s=1) + \underline{Z}_{\text{i}}(s=1) = 2\underline{Z}_{\text{d}}(s=1) \tag{9}$$

From this point of the paper, we recall $\underline{Z}_{\text{measured}}$ as:

$$\underline{Z}_{\text{measured}} = \frac{\underline{Z}_{\text{SSFR}}}{2} \tag{10}$$

Note that $\underline{Z}_{\text{measured}}$ matches up with the phase impedances of the circuits in Fig. 2.

A. Calculation of the Measured Impedance

The instantaneous voltage and current are measured for each frequency:

$$\begin{aligned} u_{\text{SSFR}}(t) &\rightarrow U_{\text{SSFR}} = \text{rms}\left(u_{\text{SSFR}}(t)\right) \\ i_{\text{SSFR}}(t) &\rightarrow I_{\text{SSFR}} = \text{rms}\left(i_{\text{SSFR}}(t)\right) \\ p_{\text{SSFR}}(t) = u_{\text{SSFR}}(t) \cdot i_{\text{SSFR}}(t) &\rightarrow P_{\text{SSFR}} = \text{avg}\left(p_{\text{SSFR}}(t)\right) \end{aligned} \tag{11}$$

The SSFR impedance, resistance and reactance for each frequency are calculated as follows:

$$\begin{aligned} Z_{\text{SSFR}}(f_k) &= \frac{U_{\text{SSFR}}(f_k)}{I_{\text{SSFR}}(f_k)} \quad ; \quad R_{\text{SSFR}}(f_k) = \frac{P_{\text{SSFR}}(f_k)}{I_{\text{SSFR}}(f_k)^2} \\ X_{\text{SSFR}}(f_k) &= \sqrt{Z_{\text{SSFR}}(f_k)^2 - R_{\text{SSFR}}(f_k)^2} \end{aligned} \tag{12}$$

Lastly, the measured impedance, resistance and reactance are calculated as:

$$\begin{aligned} Z_{\text{measured}}(f) &= \frac{Z_{\text{SSFR}}}{2} \\ R_{\text{measured}}(f) &= \frac{R_{\text{SSFR}}}{2} \quad X_{\text{measured}}(f) = \frac{X_{\text{SSFR}}}{2} \end{aligned} \tag{13}$$

B. Least-Squares Algorithm for Parameter Estimation

The analytical phase resistance and reactance of the models depends on the machine parameters **x**:

$$R(f_k) = R(\mathbf{x}, f_k) \quad ; \quad X(f_k) = X(\mathbf{x}, f_k) \tag{14}$$

with $\mathbf{x}_{\text{single-cage}} = (R_s, R_r, X_{sd}, X_m)$ for the single-cage model (restriction $X_{sd} = X_{rd}$ is used) and $\mathbf{x}_{\text{double-cage}} = (R_s, R_1, R_2, X_{sd}, X_m, X_{1d})$ for the double-cage model (restriction $X_{sd} = X_{2d}$ is used). The error functions are defined as

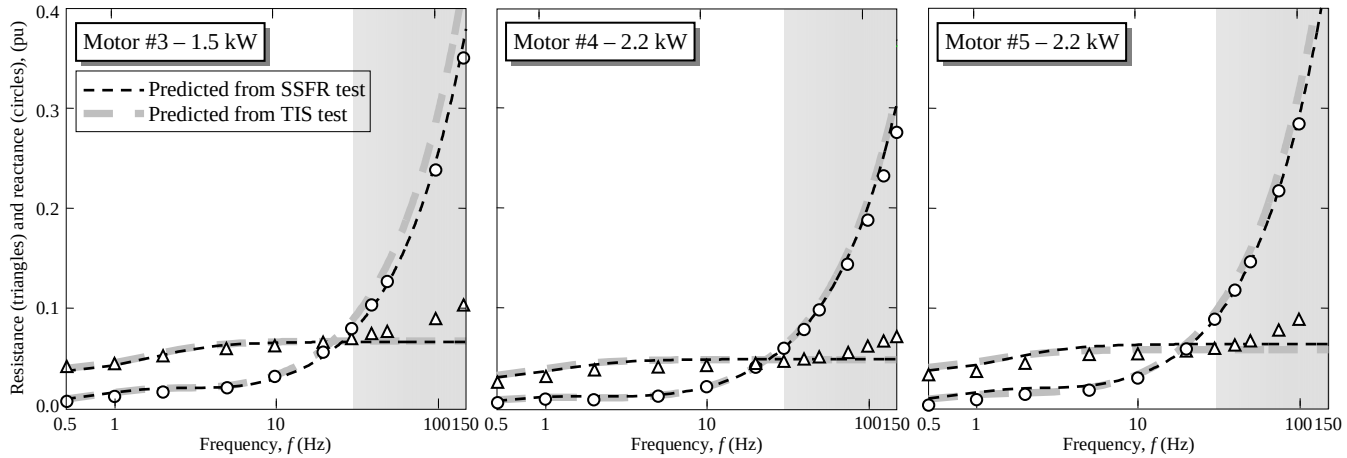

Fig. 5. SSFR test: phase resistance and reactance for motors #3, #4 and #5 measured (with marks) and predicted by the single-cage model (with broken lines).

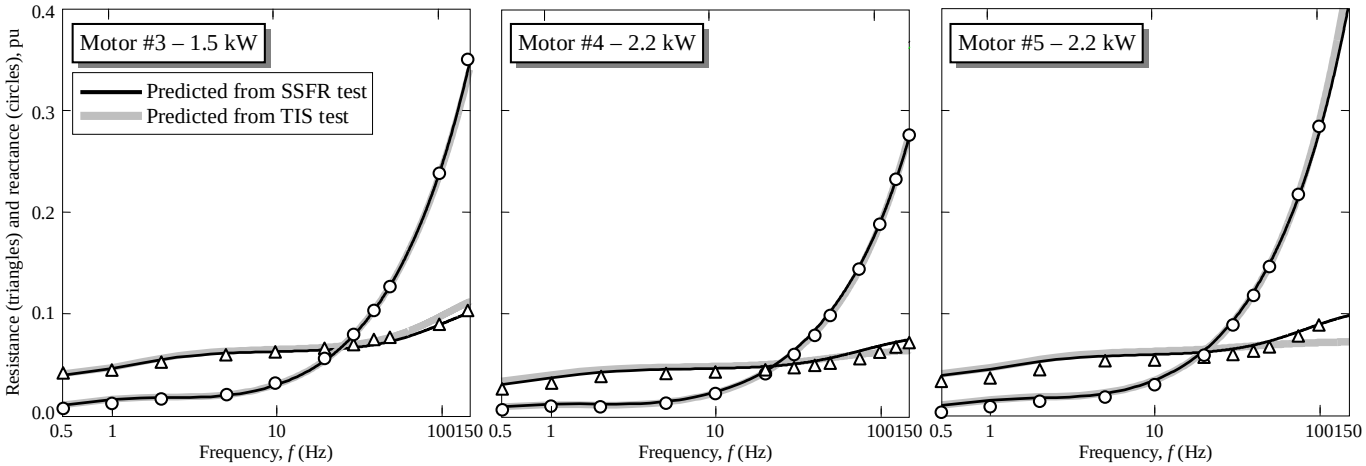

Fig. 6. SSFR test: phase resistance and reactance for motors #3, #4 and #5 measured (with marks) and predicted by the double-cage model (with solid lines).

$$\varepsilon_{\mathrm{Rk}}\left(\mathbf{x}, f_k\right)=\frac{R\left(\mathbf{x}, f_k\right)-R_{\mathrm{measured}}\left(f_k\right)}{R_{\mathrm{measured}}\left(f_k\right)}$$
$$\varepsilon_{\mathrm{Xk}}\left(\mathbf{x}, f_k\right)=\frac{X\left(\mathbf{x}, f_k\right)-X_{\mathrm{measured}}\left(f_k\right)}{X_{\mathrm{measured}}\left(f_k\right)} \quad (15)$$

and finally the parameters are estimated by solving the minimization problem by using the Matlab function `lsqnonlin` [16]:

$$\min\left\{F\left(\mathbf{x}\right)\right\}=\min\left\{\sum_{k=1}^{N}\left(\varepsilon_{\mathrm{Rk}}^2\left(\mathbf{x}, f_k\right)+\varepsilon_{\mathrm{Xk}}^2\left(\mathbf{x}, f_k\right)\right)\right\} \quad (16)$$

where N is the number of measured frequencies. Note that all estimated parameter must be positive.

C. Estimation Results Analysis

Figs. 5 and 6 summarize the laboratory data obtained with the SSFR test for motors #3, #4 and #5 in Table I. These data, computed as explained in equation (11)-(13), give the resistance, $R(f)$, (with triangles) and reactance, $X(f)$, (with circles) in each case. From these data and following the steps in Section V.B, it is possible to estimate the single- and double-cage models parameters. The obtained parameters are in Table IV.

As said before, the single-cage model is expected to be unable to explain the resistance behavior as a function of the frequency because of the skin effect (Fig. 4). For this reason, a successful estimation of the single-cage model parameters requires the use of only the low frequency data. The unused data in Fig. 5 are shaded. The resistance and reactance predicted from the estimated parameters is plotted with dashed dark lines. As expected, the single-cage model does not fit the high frequency data.

On the contrary, a good fit of the measured data and

TABLE IV
ESTIMATED PARAMETERS FOR THE SINGLE- AND DOUBLE-CAGE MODELS FROM SSFR TESTS: IN PU ($S_B = P_N$, $U_B = U_N$, $Z_B = U_B^2/S_B$)

	Single-cage model from SSFR tests				Double-cage model from SSFR tests					
	r_s	$x_{sd} = x_{2d}$	x_m	r_r	r_s	$x_{sd} = x_{2d}$	x_m	r_1	x_{1d}	r_2
Motor #3	0.0353	0.0651	1.0531	0.0358	0.0363	0.0696	1.0781	0.0331	0.0812	0.2874
Motor #4	0.0288	0.0518	1.0148	0.0241	0.0268	0.0562	1.1500	0.0254	0.0738	0.01698
Motor #5	0.0352	0.0763	1.0200	0.0337	0.0359	0.0861	1.0201	0.0314	0.1149	0.1701

predictions from the estimated parameters is obtained by considering the double-cage model, as can be seen in Fig. 6 where high frequency data has also been used in the estimation procedure.

VI. TIS TEST

Torque and current tests are measured at different speeds in the range s = 1 to s = 0 (TIS tests) for experimental validation of the previous estimated parameters. The measurements in Fig. 7 and 8 are obtained. Another set of parameters for the double-cage model is also estimated from these test data. Torque and current $\Gamma_{\text{measured}}(\omega_k), I_{\text{measured}}(\omega_k)$ measurements are made at different speeds, ω_k, for a reduced three-phase voltage.

A. Least-Squares Algorithm for Parameter Estimation

Using the analytical expressions of the torque and current at different speeds from reference [11], we obtain

$$\Gamma_{\text{measured}}(\omega_k) = \Gamma(\mathbf{x}, \omega_k) \quad ; \quad I_{\text{measured}}(\omega_k) = I(\mathbf{x}, \omega_k) \tag{17}$$

with $\mathbf{x}_{\text{single-cage}} = (R_s, R_r, X_{sd}, X_m)$ for the single-cage model (restriction $X_{sd} = X_{rd}$ is used) and $\mathbf{x}_{\text{double-cage}} = (R_s, R_1, R_2, X_{sd}, X_m, X_{1d})$ for the double-cage model (restriction $X_{sd} = X_{2d}$ is used). The error functions are defined as

$$\begin{aligned} \varepsilon_{\Gamma k} &= \frac{\Gamma(\mathbf{x}, \omega_k) - \Gamma_{\text{measured}}(\omega_k)}{\Gamma_{\text{measured}}(\omega_k)} \\ \varepsilon_{Ik} &= \frac{I(\mathbf{x}, \omega_k) - I_{\text{measured}}(\omega_k)}{I_{\text{measured}}(\omega_k)} \end{aligned} \tag{18}$$

Finally, the parameters are estimated by solving the minimization problem by using the Matlab function `lsqnonlin` [16]:

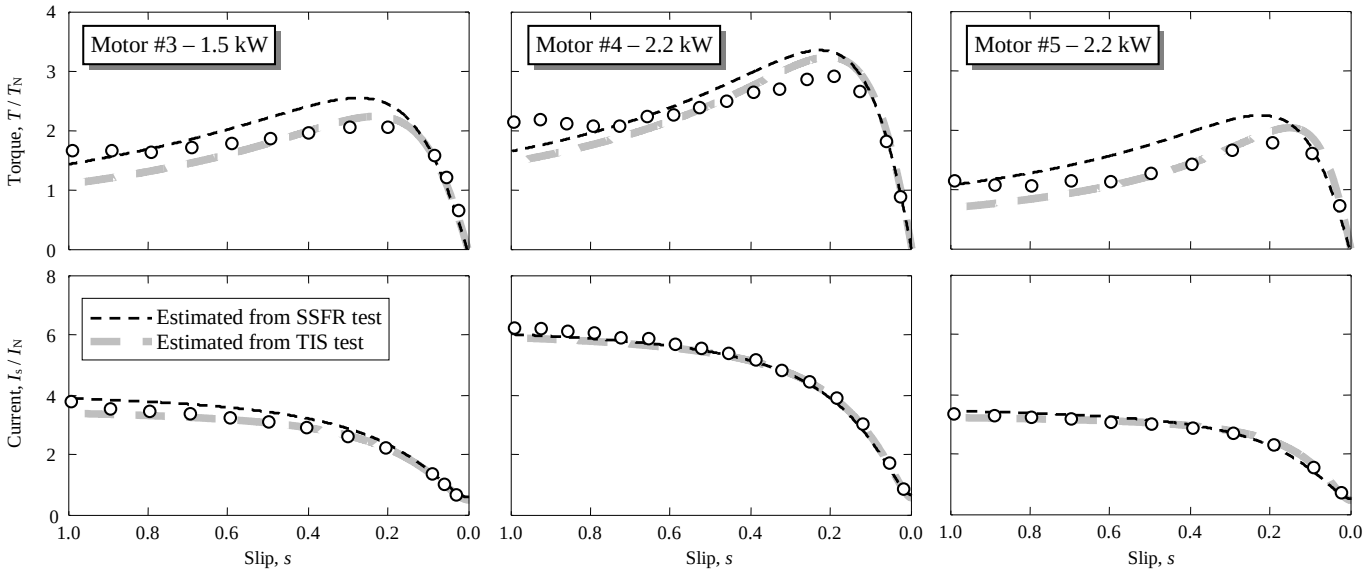

Fig. 7. TIS test: measured (with circles) and predicted by the single-cage model (lines) torque- and current-slip curves for motors #3, #4 and #5.

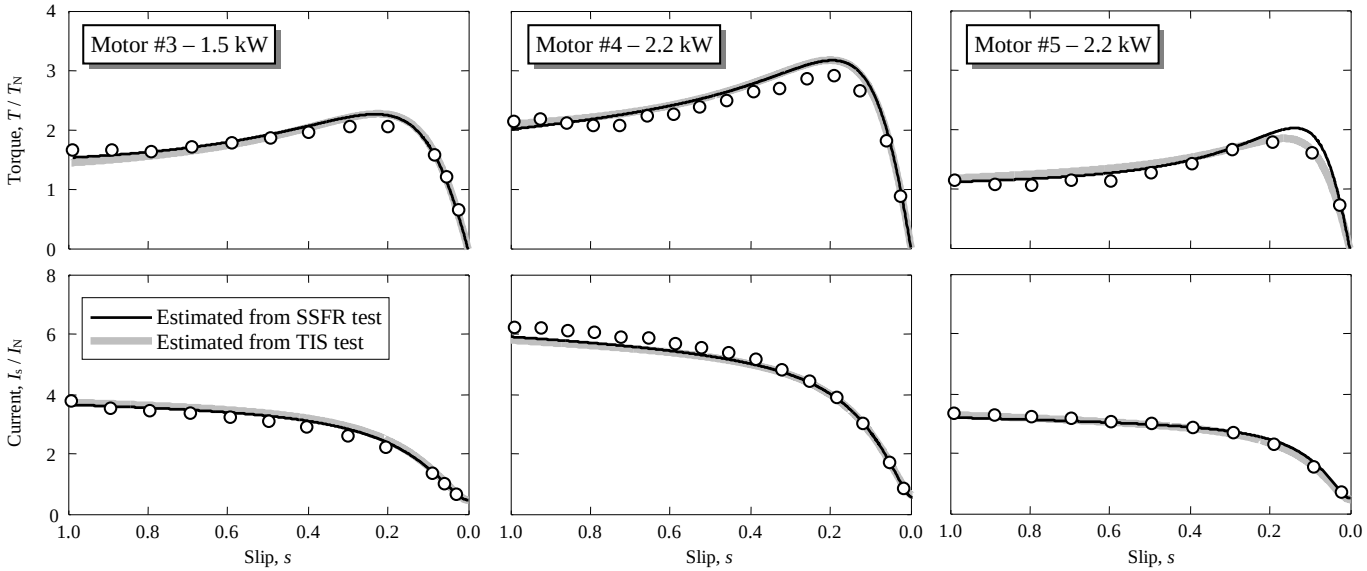

Fig. 8. TIS test: measured (with circles) and predicted by the double-cage model (with lines) torque- and current-slip curves for motors #3, #4 and #5.

TABLE V
ESTIMATED PARAMETERS FOR THE SINGLE- AND DOUBLE-CAGE MODELS FROM TIS TESTS: IN PU ($S_B = P_N$, $U_B = U_N$, $Z_B = U_B^2/S_B$)

	Single-cage model from TIS tests				Double-cage model from TIS tests					
	r_s	$x_{sd} = x_{2d}$	x_m	r_r	r_s	$x_{sd} = x_{2d}$	x_m	r_1	x_{1d}	r_2
Motor #3	0.0375	0.0757	1.0200	0.0350	0.0375	0.0650	1.0771	0.0350	0.0901	0.2989
Motor #4	0.0297	0.0534	1.2012	0.0225	0.0297	0.0592	1.2215	0.0259	0.0759	0.1072
Motor #5	0.0374	0.0833	1.0341	0.0251	0.0374	0.0895	1.0466	0.0252	0.0997	0.2357

$$\min\left\{F(\mathbf{x})\right\} = \min\left\{\sum_{k=1}^{N}\left(\varepsilon_{\Gamma k}^2(\mathbf{x},\omega_k) + \varepsilon_{Ik}^2(\mathbf{x},\omega_k)\right)\right\} \qquad (19)$$

where N is the number of measured points. Again, all estimated parameter must be positive.

B. Estimation Results Analysis

The results in Table IV were validated by comparing the predicted torque- and current-slip curves with those obtained in the laboratory (TIS tests). The circles in Figs. 7 and 8 represent the torque and stator current measured at different speeds and reduced constant voltage and rated frequency for the three tested motors. With these parameters, the predicted torque- and current-slip curves are plotted in Fig. 7 for the single-cage model, and in Fig. 8 for the double-cage model (with dark lines). Note that the curves predicted by the single-cage model do not fit the torque and current measurements whereas good accuracy is obtained with the double-cage model.

A new set of estimated parameters (shown in Table V) is obtained for the single- and double-cage models using the procedure in Section VI.A with the TIS test. With these parameters, the resistance and reactance frequency response, and the steady-state torque- and current-slip curves can be obtained for the single- and double-cage models. The results are plotted in grey lines in Figs. 5, 6, 7 and 8. As expected, only the double-cage model results fit well with the measurements.

Fig. 8 shows that even in the case of small-size motors, like motor #3, the double-cage model is necessary to correctly fit the experimental data. For large- and medium-size motors, the double-cage effect is more important, as can be observed in Fig. 3. As a consequence, it is expected that the single-cage model will be also unable to predict measured data for large- and medium-size motors.

VII. FREE-ACCELERATION TEST

The ability of the estimated double-cage parameters to predict the measured dynamic motor behavior is checked with a free-acceleration test. The Park transformed stator currents (in the synchronous reference frame) obtained from laboratory measurements are compared with those obtained from simulations.

The free-acceleration test consists in feeding the unloaded motor at a reduced voltage from standstill until steady state is reached. The electrical and mechanical parameters that characterize the test are included in Table IV.

Fig. 9 shows the Park transformed currents during the free-acceleration test. As can be seen, there is a good agreement between simulated and measured currents. The reason for this can be found in the excellent predictions of the steady-state current and torque in the whole speed range in Fig. 8.

VIII. CONCLUSION

The paper proposes a method for squirrel-cage induction

TABLE VI
LABORATORY AND SIMULATION PARAMETERS

	U_{TEST} (*) (V)	J_{SIM} (kg·m^2)	d_2 (**) (Nm/(rad/s)^2)
Motor #3	$0.52U_N$	0.115	$1.81\cdot10^{-4}$
Motor #4	$0.24U_N$	0.200	$6.00\cdot10^{-5}$
Motor #5	$0.28U_N$	0.193	$1.80\cdot10^{-4}$

(*) Obtained from the locked rotor test at rated frequency and current
(**) $\Gamma_m = d_2\cdot\omega_m^2$

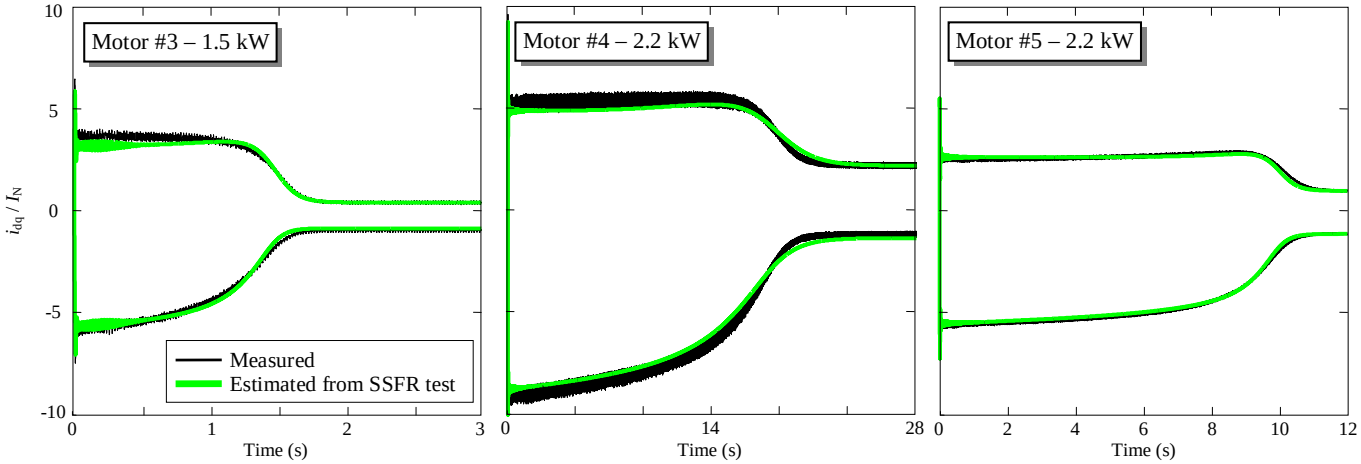

Fig. 9. Free-acceleration test: measured and predicted (double-cage) direct and quadrature stator current for motors #3, #4 and #5.

motors parameters estimation from the stator voltage and current measured in a phase-to-phase standstill frequency response (SSFR) test. The study shows that the measured equivalent resistance increases with frequency due to the skin effect. This effect only can be predicted by the double-cage model as the equivalent resistance predicted by the single-cage model remain almost constant with frequency.

The main contribution of the paper is the agreement between the measurements and the values predicted from the double-cage model parameters estimated by the SSFR test. The predicted values were compared with real measurements in two tests: (1) the steady-state torque- and current-slip curves, and (2) the dq transformed currents in a free-acceleration test. Moreover, it was demonstrated that the resistance-frequency curve is not well fitted by the single-cage model. The inability of the single-cage model to fit the resistance-frequency curve explains the predicted torque- and current-speed curve errors.

IX. Acknowledgments

The authors would like to thank Amalia Barrera and Francesc Quintana from Asea Brown Boveri, S. A., Fábrica de Motores, for providing the experimental data of the motors in Fig. 3.

X. Appendix

The symmetrical component transformation is defined by the matrix

$$\mathbf{F}=\begin{pmatrix}1 & 1 & 1\\ 1 & a^2 & a\\ 1 & a & a^2\end{pmatrix} \quad ; \quad \mathbf{F}^{-1}=\frac{1}{3}\begin{pmatrix}1 & 1 & 1\\ 1 & a & a^2\\ 1 & a^2 & a\end{pmatrix}=\frac{\mathbf{F}^{*}}{3} \tag{20}$$

Thus, the relation between three-phase voltages and currents and the homopolar, direct and inverse sequence voltages and currents is

$$\begin{pmatrix}\underline{U}_{\mathrm{AR}}\\ \underline{U}_{\mathrm{BR}}\\ \underline{U}_{\mathrm{CR}}\end{pmatrix}=\begin{pmatrix}1 & 1 & 1\\ 1 & a^2 & a\\ 1 & a & a^2\end{pmatrix}\begin{pmatrix}\underline{U}_0\\ \underline{U}_{\mathrm{d}}\\ \underline{U}_{\mathrm{i}}\end{pmatrix} \quad ; \quad \begin{pmatrix}\underline{I}_{\mathrm{A}}\\ \underline{I}_{\mathrm{B}}\\ \underline{I}_{\mathrm{C}}\end{pmatrix}=\begin{pmatrix}1 & 1 & 1\\ 1 & a^2 & a\\ 1 & a & a^2\end{pmatrix}\begin{pmatrix}\underline{I}_0\\ \underline{I}_{\mathrm{d}}\\ \underline{I}_{\mathrm{i}}\end{pmatrix} \tag{21}$$

where R can be any reference.

When only two phases of the machine are supplied (as in the test of Fig. 1), direct and inverse voltages and currents are involved. The equations that define the machine behavior (at any slip) in a phase-to-phase connection are:

$$\begin{aligned}&\underline{U}_{\mathrm{AB}}=\underline{Z}_{\mathrm{AB}}\cdot\underline{I}_{\mathrm{A}} \quad ; \quad \underline{I}_{\mathrm{C}}=0\\ &\underline{U}_{\mathrm{d}}=\underline{Z}_{\mathrm{d}}\cdot\underline{I}_{\mathrm{d}} \quad ; \quad \underline{U}_{\mathrm{i}}=\underline{Z}_{\mathrm{i}}\cdot\underline{I}_{\mathrm{i}}\end{aligned} \tag{22}$$

where $\underline{Z}_{\mathrm{d}}$ and $\underline{Z}_{\mathrm{i}}$ can be obtained from Fig. 2 by dividing R_{r} s and $2 - s$ respectively.

From (21) and the second equation in (22), we obtain

$$\underline{I}_{\mathrm{C}}=\underline{I}_0+a\cdot\underline{I}_{\mathrm{d}}+a^2\cdot\underline{I}_{\mathrm{i}}=0 \tag{23}$$

As the neutral current is null, $\underline{I}_0 = 0$, then

$$a\cdot\underline{I}_{\mathrm{d}}+a^2\cdot\underline{I}_{\mathrm{i}}=0 \;\Rightarrow\; \begin{cases}\underline{I}_{\mathrm{d}}=-a\cdot\underline{I}_{\mathrm{i}}\\ \underline{I}_{\mathrm{i}}=-a^2\cdot\underline{I}_{\mathrm{d}}\end{cases} \tag{24}$$

From (21) and the first equation in (22), we have

$$\begin{aligned}\underline{U}_{\mathrm{AB}}&=\underline{U}_{\mathrm{AR}}-\underline{U}_{\mathrm{BR}}\\ &=\left(\underline{U}_0+\underline{U}_{\mathrm{d}}+\underline{U}_{\mathrm{i}}\right)-\left(\underline{U}_0+a^2\cdot\underline{U}_{\mathrm{d}}+a\cdot\underline{U}_{\mathrm{i}}\right)\\ &=\underline{U}_{\mathrm{d}}\left(1-a^2\right)+\underline{U}_{\mathrm{i}}\left(1-a\right)\\ &=\underline{Z}_{\mathrm{d}}\underline{I}_{\mathrm{d}}\left(1-a^2\right)+\underline{Z}_{\mathrm{i}}\underline{I}_{\mathrm{i}}\left(1-a\right)\end{aligned} \tag{25}$$

By using the relations in (24), we obtain

$$\underline{U}_{\mathrm{AB}}=\underline{Z}_{\mathrm{d}}\underline{I}_{\mathrm{d}}+\underline{Z}_{\mathrm{d}}\underline{I}_{\mathrm{i}}+\underline{Z}_{\mathrm{i}}\underline{I}_{\mathrm{i}}+\underline{Z}_{\mathrm{i}}\underline{I}_{\mathrm{d}}=\left(\underline{Z}_{\mathrm{d}}+\underline{Z}_{\mathrm{i}}\right)\left(\underline{I}_{\mathrm{d}}+\underline{I}_{\mathrm{i}}\right) \tag{26}$$

and with the relation in (21)

$$\underline{I}_{\mathrm{A}}=\underline{I}_0+\underline{I}_{\mathrm{d}}+\underline{I}_{\mathrm{i}}=0+\underline{I}_{\mathrm{d}}+\underline{I}_{\mathrm{i}} \tag{27}$$

we finally have

$$\underline{U}_{\mathrm{AB}}=\left(\underline{Z}_{\mathrm{d}}+\underline{Z}_{\mathrm{i}}\right)\underline{I}_{\mathrm{A}} \tag{28}$$

where the impedance in a phase-to-phase connection (at any slip) is

$$\underline{Z}_{\mathrm{AB}}=\underline{Z}_{\mathrm{d}}+\underline{Z}_{\mathrm{i}} \tag{29}$$

If speed is null, $\underline{Z}_{\mathrm{d}}\left(s=1\right)=\underline{Z}_{\mathrm{i}}\left(s=1\right)$ and then $\underline{Z}_{\mathrm{AB}}\left(s=1\right)=2\underline{Z}_{\mathrm{d}}\left(s=1\right)$. In the test of Fig. 1, $U_{\mathrm{AB}}=U_{\mathrm{SSFR}}$ and $I_{\mathrm{A}}=I_{\mathrm{SSFR}}$.

XI. References

[1] *IEEE Standard test procedure for polyphase induction motors and generators*, IEEE Std. 112-2004, Nov. 2004.

[2] H. A. Toliyat, E. Levi, M. Raina, "A review of RFO induction motor parameter estimation techniques", *IEEE Trans. Energy Conv*, 2003, Vol.18, (2), pp. 271-283.

[3] A. Gastli, 'Identification of induction motor equivalent circuit parameters using the single-phase test', *IEEE Trans. Energy Conv*, 1999, Vol.14, (1), pp. 51-56.

[4] M. O. Sonnaillon, G. Bisheimer, C. De Angelo, G. O. Garcia, 'Automatic induction machine parameters measurements using standstill frequency-domain tests', *IET Electric Power Applicat.*, Vol. 1, no. 5, pp. 833-838, Sep. 2007.

[5] S. Moon, A. Keyhani, "Estimation of induction machine parameters from standstill time-domain data", *IEEE Trans. Industry Applications*, 1994, Vol. 30, (6), pp. 1609-1615.

[6] I. Zubia, A. Zatarain, C. Alcalde, X. Ostolaza, "In situ electrical identification method for induction wind generators", *IET Electric Power Applications*, 2011, Vol. 5, No. 7, pp. 549-557.

[7] L. Peretti, M. Zigliotto, "Automatic procedure for induction motor parameter estimation at standstill", *IET Electric Power Applications*, 2012, vol. 6, no. 4, pp. 214-224.

[8] C. Kwon, S. D. Sudhoff, "Genetic algorithm-based induction machine characterization procedure with application to maximum torque per amp control", *IEEE Trans. Energy Conv*, 2006, vol. 2, no. 2, pp. 405-415.

[9] J. R. Willis, G. J. Brock, J. S. Edmonds, 'Derivation of induction motor models from standstill frequency tests', *IEEE Trans. Energy Conv*, 1989, vol. 4, no. 4, pp. 608-615.

[10] F. Córcoles, J. Pedra, M. Salichs and L. Sainz: 'Analysis of the induction machine parameter identification', *IEEE Trans. Energy Conv*, 2002. vol. 17, no. 2, pp. 183-190.

[11] D. W. Novotny and T. A. Lipo, *Vector Control and Dynamics of AC Drives*. New York: Oxford University Press Inc., 1996, pp. 186-187.

[12] J. Pedra, F. Córcoles, 'Double-cage induction motor parameters estimation from manufacturer data', *IEEE Trans. Energy Conv*, 2004, vol. 19, no. 2, pp. 310-317.
[13] J. Pedra, 'On the determination of induction motor parameters from manufacturer data for electromagnetic transient programs', *IEEE Trans. Power Systems*, vol. 23, no. 4, November 2008, pp. 1709-1718
[14] J. Pedra, I. Candela, and L. Sainz, "Modelling of squirrel-cage induction motors for electromagnetic transient programs," *IET Electric Power Applicat.*, vol. 3, no. 2, pp. 111-122, Mar. 2009.
[15] Ll. Monjo, F. Córcoles, J. Pedra, "Saturation effects on torque- and current-slip curves of squirrel-cage induction motors", *IEEE Trans. Energy Conv*, 2013, vol. 28, no. 1, pp. 243-254.
[16] The MathWorks, Inc., *Matlab 7.9 (2009b)*. Natick, MA: 2009.